Trabajos de Geología, Universidad de Oviedo, 30 : 107-113 (2010)

Magnetic fabrics in cleaved marls and their link to deformation processes (Southern Pyrenees, Spain)

B. Oliva-Urcia[1*], E. L. Pueyo[2], J. C. Larrasoaña[3], A. Gil[4], P. Mata[5], J. M. Parés[1], A. M. Schleicher[1]

[1]*University of Michigan, 1100 N. Univ. Ave., Michigan 48105, USA.*

[2]*Instituto Geológico y Minero de España, Unidad de Geología y Geofísica, Spain.*

[3]*Instituto de Ciencias de la Tierra Jaume Almera, CSIC, Barcelona, Spain.*

[4]*Universidad de Zaragoza, Spain.*

[5]*Universidad de Cadiz, Ciencias del Mar, Spain.*

[*]*e-mail: boliva@unizar.es*

Abstract: RT-AMS ellipsoids from Upper Cretaceous carbonate rocks in the Southwestern Pyrenees exhibit an unusual orientation for rocks within a well-cleavage domain: neither do all sites show the maximum axes in the intersection lineation nor are the minimum axes at the pole of the cleavage plane. The study of the subfabrics (LT-AMS and AARM) indicates that the paramagnetic grains (phyllosilicates) respond to a layer parallel shortening, with the minimum axis perpendicular to S_0. On the other hand, the ferromagnetic grains (magnetite) orient in relation to the strain field, which also produces the cleavage domain. The maximum axes of the ferromagnetic ellipsoids have a horizontal NNE-SSW direction. An extended version of this paper is published in Oliva-Urcia *et al.* (2009).

Keywords: magnetic fabrics, RT-AMS, LT-AMS, AARM, cleavage domain, Southern Pyrenees.

Magnetic fabrics analyses (RT-AMS: Room Temperature Anisotropy of the Magnetic Susceptibility) have been used since the fifties (Graham, 1954) in order to assess the petrofabric of rocks since for most minerals crystallography determines both grain shape and AMS (Borradaile and Jackson, 2004). One of the goals of RT-AMS is to obtain the strain ellipsoid where few or no strain markers are present, since the magnetic fabric ellipsoid and the strain ellipsoid overlap (Kligfield *et al.*, 1981). In this work we report a detailed analysis of the subfabrics of remagnetized Upper Cretaceous rocks at 9 sites from the western side of the South Pyrenean Zone (Internal Sierras, figure 1), where a spaced disjunctive cleavage domain, caused by pressure solution and solution transfer, is well developed on a regional scale (Choukroune, 1976). The total fabric (RT-AMS) does not follow the expected orientation for this tectonic setting: neither do all sites show the maximum axes in the intersection lineation (L1) nor are the minimum axes at the pole of the cleavage plane. The subfabric study allows us to separate the total fabric (the contribution of paramagnetic, ferromagnetic and diamagnetic grains) from the paramagnetic (LT-AMS: Low Temperature AMS) and the ferromagnetic (AARM: Anisotropy of the Anhysteretic Remanent Magnetization) subfabrics to understand their origin and their relationship with

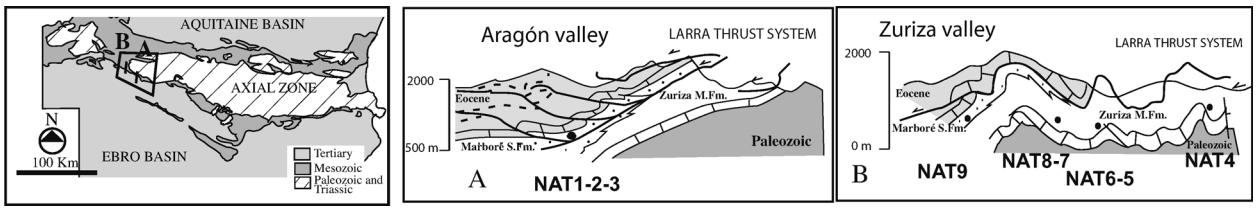

Figure 1. Location of the 9 sites in the thin-skin thrust system of the Internal Sierras, South Pyrenean Zone. Cross sections from Teixell and García-Sansegundo (1994).

the tectonic setting. In addition, optical observations and chemical qualitative analyses with the Scanning Electron Microscope (SEM) together with High-resolution X-ray Texture Goniometry (HXTG) were performed in selected samples.

Methods

Samples (10 cores per site) were taken in the field with a portable water-refrigerated drill machine. 25 to 30 standard specimens were cut in the laboratory for each site. Room Temperature AMS (RT-AMS) analyses were performed in the magnetic fabrics laboratory of the University of Zaragoza using a KLY3 Kappabridge (AGICO). Three axes define the susceptibility ellipsoid: maximum (K_{max}), intermediate (K_{int}) and minimum (K_{min}). Other parameters that give information about the shape and degree of magnetic fabric development are: the magnetic lineation ($L = K_{max}/K_{int}$) and the magnetic foliation ($F = K_{int}/K_{min}$). The corrected anisotropy degree, *P'* shows the intensity of the preferred orientation of minerals (total eccentricity), and the parameter *T* is the shape parameter, varying between prolate ($0 > T > -1$) and oblate ellipsoids ($0 < T < 1$). *P'* and *T* parameters are defined as in Jelínek (1981).

Low Temperature AMS (LT-AMS) and the Anisotropy of the Anhysteretic Remanence Magnetization (AARM) analyses were done in the paleomagnetic laboratory of the University of Michigan. The LT-AMS was analyzed using a SI2B susceptometer with an internal coil frequency of 19.2 kHz (Sapphire Instruments). Samples were immersed in liquid nitrogen (77 K during 30 min) and the AMS tensor was determined after 6 positions, measuring every position twice. The enhancement of the paramagnetic fabric at low temperatures follows the Curie-Weiss law: $X_p = C/(T-T_c)$ (see Parés and Van der Pluijm, 2002 for more details).

The AARM was analyzed using a SI-4 AF demagnetizer (Sapphire Instruments). Samples are subjected to an AF demagnetization of 100 mT peak field in one position while a 0.05 mT field is applied in a window of 5-60 mT. This procedure is performed in 9 positions for every sample, the remanent magnetization being measured for every position in a 2G-cryogenic magnetometer. The anisotropy tensor is calculated by the least-squares method (Girdler, 1961). The principal axes of the ellipsoids were displayed on stereographic projections.

Results

Magnetic Tensor Parameters (Km, P', T)

RT-AMS: bulk susceptibility values (K_m) range between 150-300×10^{-6} (SI), see table 1, which is

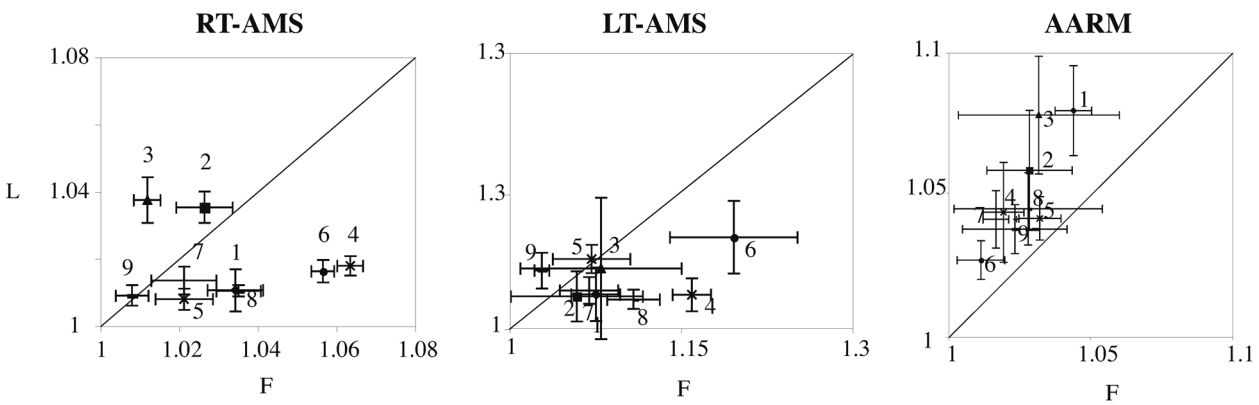

Figure 2. Flinn diagrams showing the shape of the magnetic ellipsoid for all three fabrics (Oliva-Urcia *et al.*, *submitted*).

RT-AMS

Site	Kmean (x10exp-6)	L	F	P'	T	Kmax (D&I)	Kint (D&I)	Kmin (D&I)
NAT1	182,39	1,0106	1,0344	1,0480	0,5265	220,09	310,05	71,80
NAT2	290,79	1,0353	1,0265	1,0632	-0,1514	30,09	280,66	125,22
NAT3	237,68	1,0374	1,0120	1,0521	-0,5079	33,05	297,43	129,46
NAT4	190,06	1,0178	1,0636	1,0870	0,5542	81,71	291,16	199,09
NAT5	229,93	1,0079	1,0214	1,0307	0,4381	291,14	197,19	56,67
NAT6	168,09	1,0162	1,0566	1,0775	0,5526	284,13	190,12	63,72
NAT7	233,19	1,0135	1,0213	1,0359	0,1884	59,21	321,18	196,62
NAT8	230,31	1,0104	1,0352	1,0484	0,5301	73,17	335,25	194,60
NAT9	153,74	1,0090	1,0082	1,0175	-0,0451	266,02	175,56	353,33

LT-AMS

	Kmean (x10exp-6)	L	F	P'	T	Kmax (D&I)	Kint (D&I)	Kmin (D&I)
NAT1	636,1933	1,0364	1,0756	0,3825	1,1361	282,15	185,23	36,65
NAT2	524,8657	1,0342	1,0590	0,2210	1,0920	327,12	229,29	80,64
NAT3	534,9500	1,0649	1,0801	0,2127	1,1537	314,12	238,13	102,77
NAT4	779,0900	1,0360	1,1596	0,4776	1,1919	101,47	302,41	203,10
NAT5	748,5167	1,0751	1,0720	-0,0564	1,1532	304,02	214,28	37,63
NAT6	654,1944	1,0988	1,1962	0,3247	1,3153	310,01	215,26	44,64
NAT7	662,8542	1,0406	1,0697	0,2521	1,1028	308,18	45,21	184,60
NAT8	725,3500	1,0311	1,1086	0,5385	1,1429	307,14	43,28	192,55
NAT9	491,4083	1,0624	1,0284	-0,3489	1,0924	302,05	38,36	210,54

AARM

	mA/m	L	F	P	T	Kmax (D&I)	Kint (D&I)	Kmin (D&I)
NAT1	5,5156	1,0800	1,0430	1,1270	-0,2710	25,04	295,17	129,78
NAT2	23,9812	1,0580	1,0280	1,0913	-0,3149	37,13	235,75	320,08
NAT3	15,1643	1,0780	1,0310	1,1614	-0,3106	28,03	300,24	07,76
NAT4	6,6393	1,0430	1,0190	1,0640	-0,3610	67,81	225,06	317,04
NAT5	19,6949	1,0410	1,0320	1,0752	-0,1270	196,26	5,64	105,03
NAT6	10,0652	1,0270	1,0110	1,0388	-0,4230	217,29	119,09	6,65
NAT7	12,5535	1,0410	1,0160	1,0588	-0,4059	53,20	144,06	252,67
NAT8	10,5323	1,0450	1,0280	1,0745	-0,3193	74,14	342,04	248,77
NAT9	10,0070	1,0510	1,0260	1,0621	-0,3032	212,22	70,64	307,09

Table 1. Values of K_m, L, F, P'/P and T and the orientation of the three axes of the ellipsoid for RT-AMS, LT-AMS and AARM.

typical for marls, fine grain sandstones and marly-limestones, where the paramagnetic fabric seems to be the dominant contributing factor although some ferromagnetic carriers may also contribute. The bulk susceptibility shows a relatively narrow range for the corresponding corrected anisotropy degree values (P'), which range between 1.01 and 1.09. The predominant shape of the ellipsoid is oblate (Fig. 2) (except for sites 2, 3 and 9). Sites 4 and 6 largely show the more developed fabric followed by 8 and 1, whereas 1, 2 and 9 are the only ones with a prolate ellipsoid.

LT-AMS: the mean values of the susceptibility at low-temperature range between 500-800×10^{-6} (SI), table 1. The enhancement of the bulk susceptibility at low temperature is between 1.8 and 4 times the susceptibility at room temperature. The shape of the ellipsoid is oblate (Fig 2). There is a correspondence between the increase in the anisotropy degree (P) and the oblateness of the ellipsoid (T). The anisotropy degree (P) is high at lower temperature as expected (see Parés and Van der Pluijm, 2002) with respect to the corrected anisotropy degree at room temperature.

AARM: in contrast to the shape of the ellipsoid at LT, T values for the AARM indicate a prolate shape at all sites (Fig. 2 and Table 1). The prolate shape is typical for magnetite grains with grain size larger than single domain (Borradaile *et al.*, 1999). The intensity of the AARM varies between 5 to almost 30 mA/m.

The directional characteristics of the ellipsoids (RT-AMS, LT-AMS and AARM) and paramagnetic fabric strength (HXTG) are listed below:

RT-AMS: all sites show well-developed fabrics in terms of grouping of axes in clusters, except for sites

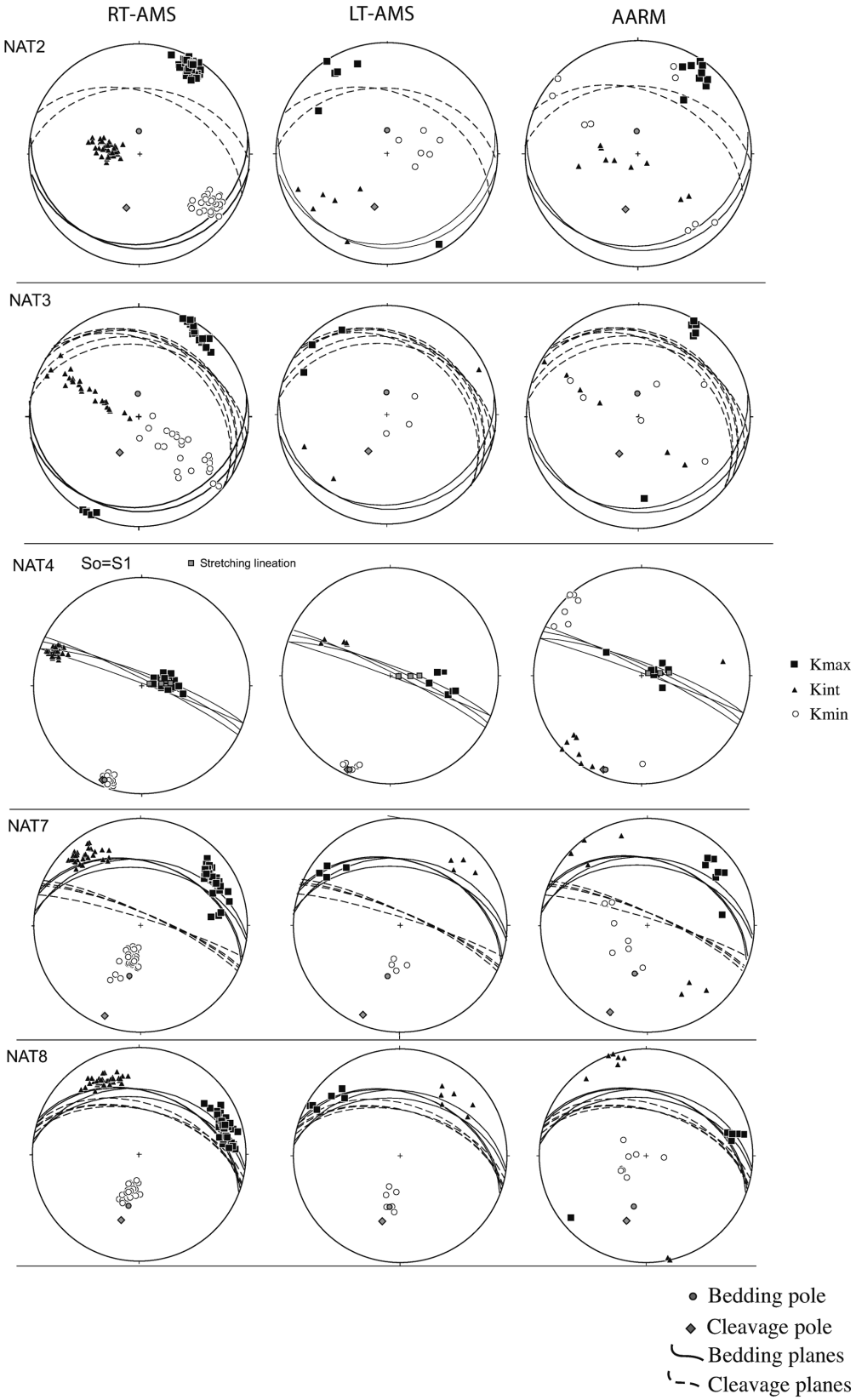

Figure 3. Examples of stereographic projections of the axes of the magnetic ellipsoids. All projections are lower hemisphere and equal area (Oliva-Urcia *et al.*, *submitted*).

2, 3 and 9 (Fig. 3). The K_{min} axes tend to cluster around the pole of the bedding plane regardless of the angle between the bedding and the cleavage planes. K_{max} and K_{int} axes tend to lie on the bedding plane or K_{max} lie on the horizontal plane (sites 1, 2 and 3). Generally, K_{max} axes tend to be closer either to the intersection lineation (L1), or along a NE direction.

LT-AMS: the orientation of the ellipsoid remains similar in all the sites. K_{max} axes cluster around the intersection lineation (L1), indicating that the long axes of the ellipsoid are both on the bedding and the cleavage planes (Fig. 3). Only in one case do K_{max} axes coincide with the stretching lineation as recorded in the field (site 4). Interestingly, for sites situated in a well-developed cleavage area, K_{min} axes cluster around the bedding pole (except in site 9) whereas K_{int} axes cluster or tends to cluster on the bedding plane. In sites 1, 2 and 3 the grouping is less obvious but tends to be near the bedding pole except for the last mentioned.

The HXTG technique provides more information about the preferred orientation in the stacking of the phyllosilicates layers (mica and chlorite). The greater the m.r.d. (multiple of random distribution; Van der Pluijm *et al.*, 1994) value, the better aligned the clay fabric. The strength in the stacking of the layers changes both from site to site and also between the mica and chlorite minerals. A similar range of variations has been found in other shale-slate transitions with cleavage development in the slates (e.g. Ho *et al.*, 1994). Overall, the mica minerals have a stronger fabric than the chlorite crystals, except for sites 4, 5 and 6, where m.r.d values for both minerals are very similar. The strongest fabric development in micas was determined at locality 4-1a (m.r.d. = 6.65).

AARM: the orientation of the ellipsoid of the remanent magnetization remains fairly constant, especially for the K_{max} axes, which cluster on the bedding plane and always along a NNE or SSW direction (Fig. 3). In sites 1, 2 and 3, K_{max} axes fall between the bedding and the cleavage planes, in the horizontal plane when *in situ* projection is used, in the other sites K_{max} axes are always pseudo-parallel to the bedding plane. Except for site 4, the other sites show K_{max} axes close to the horizontal plane (less than 20º). The K_{min} axes tend to be either around the bedding pole (7) or closer to the bedding pole (1, 8), forming a girdle with K_{int} (2, 3, 6 and 9) or interchanging with K_{int} (4 and 5). In the latter case, K_{min} axes cluster near the bedding plane, whereas K_{int} axes cluster around the bedding pole.

Carriers of the fabric

Phyllosilicates

The phyllosilicates observed under the SEM are basically micas and Interleaved Phyllosilicate Grains (IPG), chorite/mica being the most frequent. They are the carriers of the LT-AMS subfarbic. IPG are the result of the stacking of layers (from angstroms to microns) of phyllosilicates on (001) planes.

Iron-oxides

Rock magnetism and paleomagnetic analyses show that magnetite is the main carrier of the AARM. Concerning the nature and relative contribution of the magnetic mineralogy: 1) the acquisition of isothermal remanent magnetization (IRM) shows the presence of a soft magnetic mineral; 2) IRM of three components, giving the result of a soft magnetic carrier with unblocking temperatures of 580 ºC, typical for magnetite; 3) low temperature curves with the Verwey transition at 120 K, also typical of magnetite (see Oliva-Urcia and Pueyo, 2007 for more details). The hysteresis loops indicate 60-70% of paramagnetic material present in the samples as expected from the bulk susceptibility distribution. In addition to all these data, it is necessary to mention the presence of a widespread remagnetization in the formations of the same age. The remagnetization is postfolding with an unblocking temperature range of 250-450 ºC and is carried by magnetite. The remagnetization was characterized in 80% of the studied sites, although a primary component remains in 30% of the studied sites (see Oliva-Urcia and Pueyo, 2007 for more details).

Discussion

Two types of sites can be defined considering this data set and the orientation of the ellipsoids:

Type I: sites where the RT-AMS coincides with LT-AMS but is different from AARM ellipsoids, such as in sites 4, 5 and 6. These sites show the highest chlorite m.r.d. values. In these sites, K_{min} axes are at the pole of the bedding plane. K_{max} axes are parallel to the intersection lineation except for site 4, where they are parallel to a vertical stretching lineation, measured in the field.

Type II: sites where RT-AMS coincides with AARM but is different from LT-AMS ellipsoid. Sites 1, 2, 3, 7 and 8 fit in this group although two subgroups can be defined here: IIa) sites where K_{max} is on the bedding plane (7 and 8), and IIb) where K_{max} is between

the bedding and the cleavage plane (1, 2 and 3) on the horizontal plane when *in situ* coordinates are used. The exception is site 9, where the RT-AMS ellipsoid shows an intermediate orientation between LT-AMS and AARM. AARM shows an interchange between K_{int} and K_{min} with respect to the other sites.

In most cases, LT-AMS ellipsoids have the K_{max} axes grouped perpendicular to the shortening direction in the intersection lineation (L1) and K_{min} in the bedding pole, showing no relationship with the cleavage orientation. They follow the typical fabric pattern related to layer parallel shortening (Aubourg *et al.*, 1997; Parés *et al.*, 1999; Larrasoaña *et al.*, 2004). The cleavage is developed afterwards without significant alteration of the phyllosilicate inherited magnetic fabric as in Aubourg *et al.* (1997). On the other hand, the AARM ellipsoids show a more complex relationship with the two petrofabric planes (bedding and cleavage). On the one hand K_{max} axes group on the bedding plane near the horizontal or the horizontal (*in situ* projection) except site 4 and, on the other, K_{max} axes group following a NNE-SSW direction. This orientation corresponds to the transport direction of thrusts and the lineations measured on ramps and on N-dipping cleavage planes in the tectonic setting of the area. These thrust units are prior to the development of the regional cleavage domain (Choukroune and Seguret, 1973; Teixell *et al.*, 2000). The stretching direction related to the tectonic transport direction has been postulated to interpret anomalous orientations of the RT-AMS ellipsoid and is carried for detrital titanomagnetites, whereas the phyllosilicates retain the orientation of the LPS prior to stretching; so a competition between these two fabrics occur, producing in some cases the scattering of the K_{max} axes (Aubourg *et al.*, 1991; 1995).

Conclusions

The relatively complex rock magnetic properties and deformation history of the studied rocks require a meticulous study of the subfabrics and magnetic mineralogy in order to properly interpret the petrofabric and its relationship to strain. The total fabric (RT-AMS) neither has a common pattern nor follows the typical orientation for a well-developed cleavage domain area. From this multidisciplinary approach, we can conclude:

The ferromagnetic grains (magnetite) control the low-field susceptibility (RT-AMS). There is a predominance of sites where AARM ellipsoid mimics RT-AMS. Only in 2 sites (5 and 6) does the LT-AMS coincide with the RT-AMS (probably due to the predominance of chlorite).

The preferred orientation of the paramagnetic grains is related to an early phase of syn-sedimentary compression (layer parallel shortening during the Upper Cretaceous). The ferromagnetic fabric due to magnetite is related to the shear/stretching direction, as shown by the grouping of K_{max} axes in the NNE direction.

Acknowledgements

Funding comes from the projects BTE 2002-04168, CGL2006-2289-BTE (MEC, Spain) and Geokin3DPyr (CTPR04/2005-INTERREG IIIa- European Council). Ben van der Pluijm is also acknowledged for fruitful discussions. We also thank the assistance given by the EMAL laboratory at the University of Michigan.

References

AUBOURG, C., ROCHETTE, P. and VIALON, P. (1991): Subtle stretching lineation revealed by magnetic fabric of Callovian-Oxfordian black shales (French Alps). *Tectonophysics*, 185: 211-223.

AUBOURG, C., ROCHETTE, P. and BERGMÜLLER, F. (1995): Composite magnetic fabric in weakly deformed black shales. *Phys. Earth Planet. In.*, 87: 267-278.

AUBOURG, C., FRIZON DE LAMOTTE, D., POISSON, A. and MERCIER, E. (1997): Magnetic fabrics and oblique ramp-related folding: A case study from the western Taurus (Turkey). *J. Struct. Geol.*, 19, 8: 1111-1120.

BORRADAILE, G. J., WERNER, T. and LAGROIX, F. (1999): Magnetic fabrics and anisotropy-controlled thrusting in the Kapuskasing Structural Zone, Canada. *Tectonophysics*, 302: 241-256.

BORRADAILE, G. J. and JACKSON, K. (2004): Anisotropy of magnetic susceptibility (AMS); magnetic petrofabrics of deformed rocks. *Geol. Soc. Spec. Publ.*, 238: 299-360.

CHOUKROUNE, P. (1976): Structure et évolution tectonique de la zone nord-pyrénéene: Analyse de la déformation dans une portion de la chaîne à schistosité subverticale. *Mem. Soc. Géol. Fr.*, 127: 1-116.

CHOUKROUNE, P. and SEGURET, M. (1973): *Carte Structurale des Pyrénées*. ELF-ERAP, Mission France, Boussens.

GIRDLER, R. W. (1961): The measurement and computation of anisotropy of magnetic susceptibility in rocks. *Geophys. J. Roy. Astr. S.*, 5: 34-44.

GRAHAM, J. W. (1954): Magnetic susceptibility anisotropy, an unexploited petrofabric element. *Geol. Soc. Am. Bull.*, 65, 12, 2: 1257-1258.

HO, N. C., PEACOR, D. R. and VAN DER PLUIJM, B. A. (1994): Reorientation mechanisms of phyllosilicates in the mudstone-to-slate transition at Lehigh Gap, Pennsylvania. *J. Struct. Geol.*, 17, 3: 345-356.

JELÍNEK, V. (1981): Characterization of the magnetic fabric of rocks. *Tectonophysics*, 79: 63-70.

KLIGFIELD, R., OWENS, W. H. and LOWRIE, W. (1981). Magnetic susceptibility anisotropy, strain, and progressive deformation in Permian sediments from the Maritime Alps (France). *Earth Planet. Sc. Lett.*, 55: 181-189.

LARRASOAÑA, J. C, PUEYO, E. L. and PARÉS, J. M. (2004): An integrated AMS structural, paleo- and rock-magnetic study of the Eocene marine marls from the Jaca-Pamplona basin (Pyrenees, N Spain); new insights into the timing of magnetic fabric acquisition in weakly deformed mudrocks. In: F. MARTÍN-HERNÁNDEZ, C. M. LÜNEBURG, C. AUBOURG and M. JACKSON (eds): *Magnetic fabric, methods and applications. Geol. Soc. Spec. Publ.*, 238: 127-143.

OLIVA-URCIA, B. and PUEYO, E. L. (2007): Rotational basement kinematics deduced from remagnetized cover rocks (Internal Sierras, southwestern Pyrenees). *Tectonics*, 26, TC4014, doi:10.1029/2006TC001955.

OLIVA-URCIA, B., LARRASOAÑA, J. C., PUEYO, E. L., GIL, A., MATA, P., PARÉS, J. M., SCHLEICHER, A. M. and PUEYO, O. (2009): Disentangling magnetic subfabrics and their link to deformation processes in cleaved sedimentary rocks from the Internal Sierras (west central Pyrenees, Spain). *J. Struc. Geol.,* 31: 163-176.

OLIVA-URCIA, B., PUEYO, E. L., LARRASOAÑA, J. C., GIL, A., MATA, P., PARÉS, J. M., SCHLEICHER, A. M. and PUEYO, O. (submitted): Complex magnetic subfabrics and their link to deformation processes in cleaved sedimentary rocks (Internal Sierras, Pyrenees, Spain). *Tectonophysics*.

PARÉS, J. M., VAN DER PLUIJM, B. A. and DINARÉS-TURELL, J. (1999): Evolution of magnetic fabrics during incipient deformation of mudrocks (Pyrenees, northern Spain). *Tectonophysics*, 307: 1-14.

PARÉS, J. M. and VAN DER PLUIJM, B. (2002): Evaluating magnetic lineations (AMS) in deformed rocks. *Tectonophysics*, 350: 283-298.

TEIXELL, A. and GARCÍA-SANSEGUNDO, J. (1994): *Mapa Geológico de España, Escala 1:50 000, 2ª serie, Hoja n° 118: ZURIZA*. Instituto Tecnológico Geominero de España, Madrid.

TEIXELL, A., DURNEY, D. W. and ARBOLEYA, M. L. (2000): Stress and fluid control on decollement within competent limestone. *J. Struct. Geol.*, 22: 349-371.

VAN DER PLUIJM, B. A., HO, N. C. and PEACOR, D. (1994): High-resolution X-ray texture goniometry. *J. Struct. Geol.*, 16, 7: 1029-1032.